T. J. Kriewall
Orthopaedic Products Division,
3M Company,
St. Paul, Minn. 55144

N. Akkas
Department of Civil Engineering,
Middle East Technical University,
Ankara, Turkey

D. I. Bylski
Bioengineering Program,
University of Michigan,
Ann Arbor, Mich. 48109

J. W. Melvin
Highway Safety Research Institute,
University of Michigan,
Ann Arbor, Mich. 48109

B. A. Work, Jr.
Department of Obstetrics and Gynecology,
University of Illinois,
Chicago, Ill. 60612

Mechanical Behavior of Fetal Dura Mater Under Large Axisymmetric Inflation

The nonlinear mechanical behavior of fetal dura mater was tested experimentally and compared to two published nonlinear material strain energy functions, the Mooney-Rivlin and the Skalak, Tozeren, Zarda, and Chien (STZC). The STZC constitutive relations best fit the behavior of the dura mater and were used to describe quantitatively its stiffness. Runge-Kutta numerical procedures were used to fit the theoretical data to the experimental results. The material's stiffness was positively correlated with fetal weight ($r=0.67$, $p<0.05$). *These results are discussed and directions for future research indicated.*

Introduction

Many events surrounding the birth process continue to be enigmas even in our space-age society. Although the death rate associated with the birth process in the U.S. is relatively low (1–3 per 1000 live births), half are unexplained [1]. The State Assembly on Developmental Disabilities of California estimated 30,000 to 44,000 mentally retarded individuals are added to our population annually, nearly half severely [2]. Besides the human tragedy mental and physical handicaps represent, Quilligan and Paul estimate supportive care costs 4 billion dollars annually [3]. They postulate that with more knowledge of labor and delivery, decreasing the number of cases of mental and physical handicaps by 50 percent is possible.

For example, a better understanding of fetal skull molding is needed. Unlike the rigid adult skull, fetal skull bones are flexible plates connected at their margins by soft tissue. The bones translate and flex under the forces of labor so the head can pass through the cervix and maternal pelvis. The extent of the bones' movements are limited, in part, by the soft tissue complex of the dura mater, falx cerebri and tentorium cerebelli. These are all tough, fibrous membranes surrounding the brain and attached to the inner aspects of the skull bones and its base.

Undefined limits exist to this molding process. In the case of cephalopelvic disproportion, the head is too large to safely pass through the maternal pelvis. The aforementioned mortality and morbidity statistics imply that a grey area exists in which frank disproportion may not be evident. If left to deliver vaginally, the head will pass through the canal, but molding will be severe enough to cause death or neurological deficits, a condition that cannot be accurately diagnosed today. The purpose of this research is to characterize the mechanical behavior of fetal dura mater, a nonlinear viscoelastic membrane, so that safe limits to skull molding may be better defined.

Background

The fibrous nature of soft biological tissues results in nonlinear stress-strain characteristics [4]. Adult dura is anisotropic [5]; fetal dura is assumed to be similar. Also, dura is viscoelastic. However, anisotropy and viscoelasticity can be ignored in any gross modeling effort. The general variability in adult tissue tends to overshadow the effects of fiber orientation [5]. Since birth is relatively slow or quasi-static, viscoelastic characteristics can be considered of second-order importance. Thus, in our mathematical model the dura is assumed to be incompressible, homogeneous, isotropic and nonlinearly elastic.

Skull molding is a large deformation process. Borell and Fernstrom found through intrapartum radiographs that the

Contributed by the Bioengineering Division for publication in the JOURNAL OF BIOMECHANICAL ENGINEERING. Manuscript received by the Bioengineering Division, May 15, 1981; revised manuscript received July 1982.

Table 1 Biographical data for the test material used in this investigation

Calvarium no.	Estimated gestational age (wk)	Sex	Weight(g)	Nominal Thickness (mm)	Storage temperature (°C)	Cause of death
14 – parietal left	30	F	1491	0.70	−10	Sepsis and RDS
14 – parietal right	30	F	1491	0.52	−10	Sepsis and RDS
15 – parietal right	42	F	2850	0.51	−10	Hypoplastic left heart
16 – parietal right	39	F	2922	0.75	−10	Aortic atresia
17 – parietal right	30	M	987	0.55	−10	Cystadenomtoid malformation lung
18 – parietal right	40	M	3612	0.54	−10	Diaphragmatic hernia
19 – parietal left	40	M	2550	0.44	−10	Trisomy 21 (G-G)
20 – parietal left	33	M	1783	0.52	5	Respiratory distress syndrome
21 – parietal left	30	F	1400	0.39	5	Respiratory distress syndrome

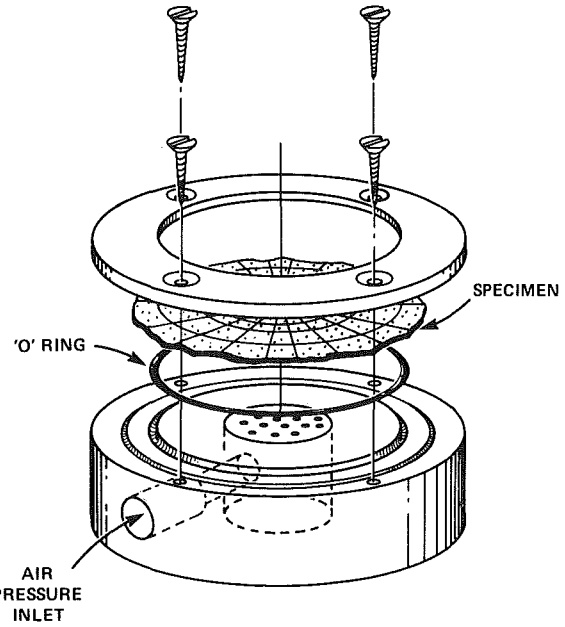

Fig. 1 The membrane is clamped into the fixture shown in the figure for the inflation test. Knurled rubber is glued to the underside of the top ring to keep the membrane from slipping during inflation.

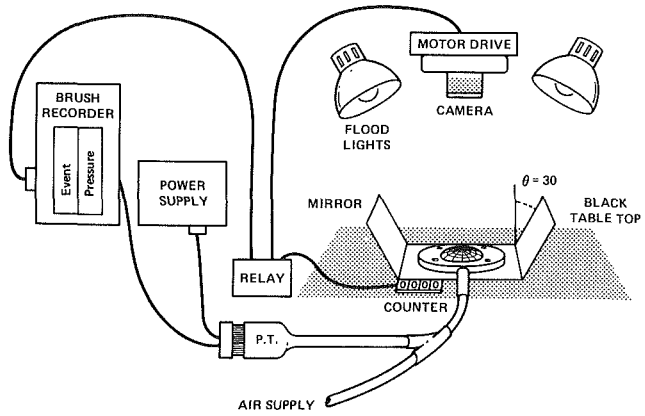

Fig. 2 A schematic representation of the experimental apparatus is shown

biparietal diameter can increase in some cases as much as 10 mm, more than a 10 percent change [6]. Therefore, modeling must include geometric nonlinearities.

The theory of nonlinearly elastic membranes undergoing large deformations is described by Green and Adkins [7], Feng and Yang [8], Yang and Feng [9], Benedict, et al. [10], and Bogen and McMahon [11].

Procedure

Dura mater was excised from calvaria of fetuses that died from causes that would not appreciably affect the development of the dura. The estimated gestational ages ranged from 30 to 42 wk; fetal masses ranged from 987 to 3612 g. Table 1 lists data regarding the fetuses and their dura.

After excision, the dura was immediately stored in 0.9 N saline solution. Some specimens were acquired prior to test development, and so were frozen. The others were refrigerated at 5°C until testing could be performed.

Circular specimens 60 mm in diameter were cut from the dura sheets. A specimen was mounted in an aluminum clamp with inner and outer diameters of 36 mm and 71 mm (Fig. 1). To secure the dura, the top portion of the clamp has a ring of hard knurled rubber on its underside. In addition, the bottom portion has two grooves: the inner groove contains an O-ring, and the edge of the membrane is secured in the outer groove when the fixture is assembled. Thirteen symmetric holes in the base of the fixture provide air flow for inflation.

Two aluminum front surface mirrors, directly opposed, were oriented 30 deg from the vertical (Fig. 2). A motor-driven 35-mm single-lens reflex camera was mounted above

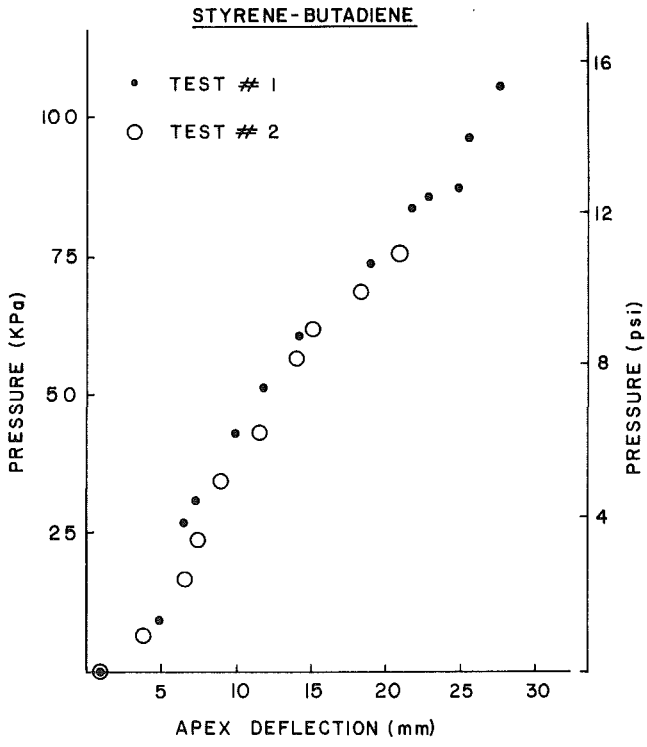

Fig. 3 Two samples from the same sheet of styrene – butadiene, a nonlinear rubber, were tested for experimental reproducibility purposes. The measured responses were within the expected variations in material behavior. The solid dots represent the first test and the open circles the second test.

the fixture. The event of a photograph was marked via the shutter release, which was connected through a relay to one channel of a Brush strip-chart recorder. Inflation pressure, measured with a National Semiconductor LX1730GB pressure transducer, was recorded on the second channel. Y-

configuration tubing connected the inflation fixture, pressure transducer, and air supply.

Just prior to testing, the dura specimen was allowed to warm to room temperature (23°C). Its thickness was measured with a dial indicator in at least four randomly selected locations. The measurements were taken upon initial contact with the membrane, before tissue compression occurred. The dura was kept moist with saline solution at all times.

A latex sheet 0.094 mm thick was glued to the O-ring with cyanoacrylate adhesive. The dura was then glued at its perimeter to the latex sheet to prevent air from permeating the porous dura.

A circumferential grid pattern was applied to the dura with a rubber stamp and water-insoluble drawing ink (Fig. 1). The stamp was aligned with marks on the fixture which, together with a calibration hemisphere, allowed for the three-dimensional grid point reconstruction from the photographs.

Two zero pressure reference frames were photographed after the calibration shots. The pressure was increased in slow, discrete, roughly equal increments. At each increment a photograph was taken after membrane motion stopped. This procedure was repeated until the dura ruptured, usually between 200 to 300 KPa (30 to 40 psi). The average inflation rate was less than 7 KPa/s (1 psi/s). About fifteen photographs were taken per test.

After the test the grid points were digitized. The three-dimensional coordinates were then reconstructed by a technique called Direct Linear Transformation [12].

Two tests were performed to check the reproducibility of the experimental results. Styrene-butadiene rubber was chosen because it had been the subject of a similar study by Wineman [13]. Figure 3 demonstrates that two separate sheets from the same stock of material generated virtually identical load-deflection curves. Therefore, any differences we found in the biological material would likely be inherent in the material, not in the test protocol.

To determine if the latex sheet affected the dura loading deflection curve, we studied the latex sheet without dura. The latex expanded to an apex deflection of 2.5 cm by applying only 3.5 KPa (0.5 psi). Thus, the compliance of the latex is significantly greater than that of the dura and did not affect the results.

Analysis

Membrane inflation tests have been performed on both nonbiological materials [13] and biological materials [14, 15]. The geometry of a membrane in its initial and deformed configurations is shown in Fig. 4. The loading and geometry are axisymmetric. The point Q defined by the coordinates (r, z) in the initial configuration is displaced to the point Q' defined by (ρ, ξ) in the deformed configuration. The principal directions of the stresses and stretch ratios at each point on the membrane reference surface are in the meridional, circumferential, and normal directions. The stretch ratios in the meridional and circumferential directions will be denoted by λ_1, and λ_2, respectively. By definition they are

$$\lambda_1 = \frac{dS}{ds} \tag{1}$$

$$\lambda_2 = \frac{\rho}{r} \tag{2}$$

where dS and ds are the meridional arc lengths in the deformed and undeformed configurations.

From incompressibility, the stretch ratio in the normal direction, λ_3, can be obtained from the relation

$$\lambda_1 \lambda_2 \lambda_3 = 1 \tag{3}$$

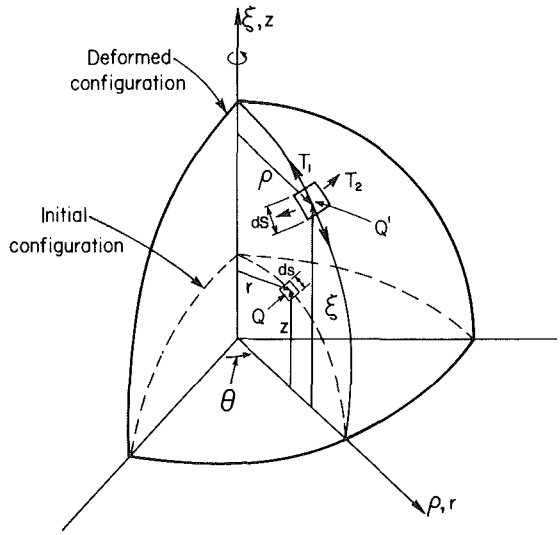

Fig. 4 Stretch ratios, λ, are defined by comparing the axisymmetric membrane in its initial and deformed configurations as point Q moves to Q'. T_1 and T_2 are the membrane forces in the aeridional and circumferential directions, respectively. The points Q and Q' are defined by their coordinates r, z, θ and ρ, ξ, θ.

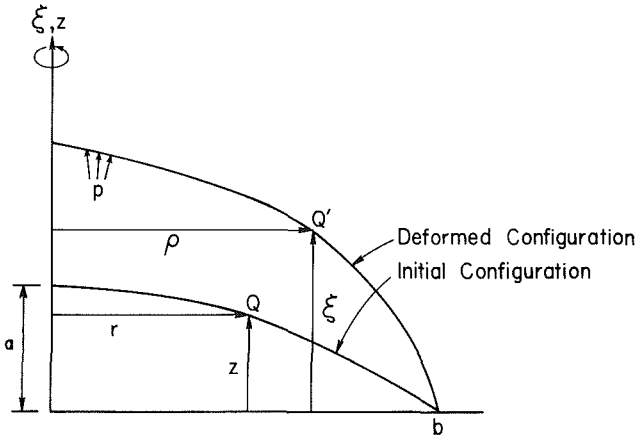

Fig. 5 In order that the numerical procedures could satisfactorily account for the behavior of the membrane, an initial apex deflection, a, had to be specified for $p = 0+$ where p is the pressure. The radius of the membrane at the equator is b.

The initial experimental configuration of the dura was meant to be flat. However, when this supposedly flat membrane was subjected to a negligibly small pressure, a sudden small deformation took place. This is due to the fact that the slope of the stress-strain relation of soft biological tissues at small strain remains very small [16]. Moreover, measuring the length at rest of a strip of soft tissue is always very difficult. For this reason, the initial reference configuration of the dura is represented as a shallow spherical cap as shown in Fig. 5. The equation of this reference configuration is

$$z = a(1 - r^2/b^2) \tag{4}$$

As shown in Fig. 5, a is the initial height and b is the radius of the membrane. The problem is to determine the deformed configuration when the initial configuration and the uniform pressure are given. A similar problem has been solved by Pujara and Lardner [17].

Consider an element cut from the membrane of revolution of Fig. 4 in the deformed configuration. The force balance equations in the principal directions are as follows:

$$\frac{dT_1}{d\rho} + \frac{1}{\rho}(T_1 - T_2) = 0 \tag{5}$$

$$K_1 T_1 + K_2 T_2 = p. \tag{6}$$

Here, T_1 and T_2 are the membrane forces in the principal directions, K_1 and K_2 are the principal curvatures, and p is the uniform pressure in the normal direction acting on the deformed membrane. Writing the principal curvatures K_1 and K_2 in terms of the principal stretch ratios λ_1 and λ_2, substituting them in equations (5), (6), and transforming the resulting equations to the initial configuration, we obtain the following equilibrium equations:

$$T_1' = -\frac{\eta}{r\lambda_2}(T_1 - T_2), \tag{7}$$

$$\frac{T_1}{\bar{\lambda}_1^2[\bar{\lambda}_1^2 - \eta^2]^{1/2}}(\bar{\lambda}_1'\eta - \bar{\lambda}_1\eta') + \frac{T_2}{r\bar{\lambda}_1\lambda_2}[\bar{\lambda}_1^2 - \eta^2]^{1/2} = p, \tag{8}$$

in which

$$(\ )' \equiv \frac{d(\ )}{dr}, \eta = \rho'$$

and

$$\bar{\lambda}_1 = \lambda_1[1 + (z')^2]^{1/2} = \lambda_1\Omega.$$

where

$$\Omega \equiv [1 + (z')^2]^{1/2} \tag{9}$$

To the equilibrium equations (7) and (8), a compatibility condition must be added

$$\lambda_2' = \frac{1}{r}(\eta - \lambda_2). \tag{10}$$

In their most general forms, the constitutive equations will be assumed to express the membrane forces T_1 and T_2 in terms of the principal stretch ratios λ_1 and λ_2, as follows

$$T_1 = F(\lambda_1, \lambda_2), \quad T_2 = G(\lambda_1, \lambda_2). \tag{11}$$

Substituting equation (11) into the equilibrium equations (7), (8), we obtain

$$\bar{\lambda}_1' = \frac{\Omega}{\partial F/\partial\lambda_1}\left[-\frac{\bar{\lambda}_1(F-G)}{r\lambda_2\Lambda} - \frac{\partial F}{\partial\lambda_2}\left(\frac{\bar{\lambda}_1}{r\Lambda} - \frac{\lambda_2}{r}\right) + \frac{\partial F}{\partial\lambda_1}\frac{\bar{\lambda}_1\Omega'}{\Omega^2}\right], \tag{12}$$

$$\Lambda' = -\frac{G\bar{\lambda}_1}{rF\lambda_2}(\Lambda^2 - 1) + \frac{p}{F}\bar{\lambda}_1\Lambda[\Lambda^2 - 1]^{1/2} \tag{13}$$

in which $\Lambda = \bar{\lambda}_1/\eta$. The compatibility condition (10) can be written as

$$\lambda_2' = \frac{\bar{\lambda}_1}{r\Lambda} - \frac{\lambda_2}{r}. \tag{14}$$

The three equations (12)–(14) are sufficient to determine the three unknowns λ_1, λ_2 and Λ for a given pressure p.

By a discussion similar to that in Green and Adkins [7] and Wineman [13], at $r = 0$

$$\begin{aligned} \lambda_1 &= \bar{\lambda}_1 = \lambda_2 = \eta = \lambda_0, \Lambda = 1, \\ \lambda_1' &= \bar{\lambda}_1' = \lambda_2' = \eta' = \Lambda' = 0, \end{aligned} \tag{15}$$

where λ_o, the stretch ratio at the apex, is assumed to be known in the numerical procedure used in the solution. The boundary condition at $r = b$ is $\lambda_2 = 1$.

In studies related to elasticity of bodies capable of finite deformation, an approach commonly used is to postulate the form of an elastic potential, or strain energy function [7]. A discussion of various functions can be found in Crisp [18] and Fung [4]. The constitutive equations selected for the present study are the Mooney-Rivlin material model [7] and the Skalak, Tozeren, Zarda and Chien [19] material model.

For the Mooney-Rivlin model, the constitutive relations are

$$T_1 = \frac{2hC_1}{\lambda_1\lambda_2}(\lambda_1^2 - \bar{\lambda}_1^2\bar{\lambda}_2^2)(1 + \alpha\lambda_2^2), \tag{16}$$

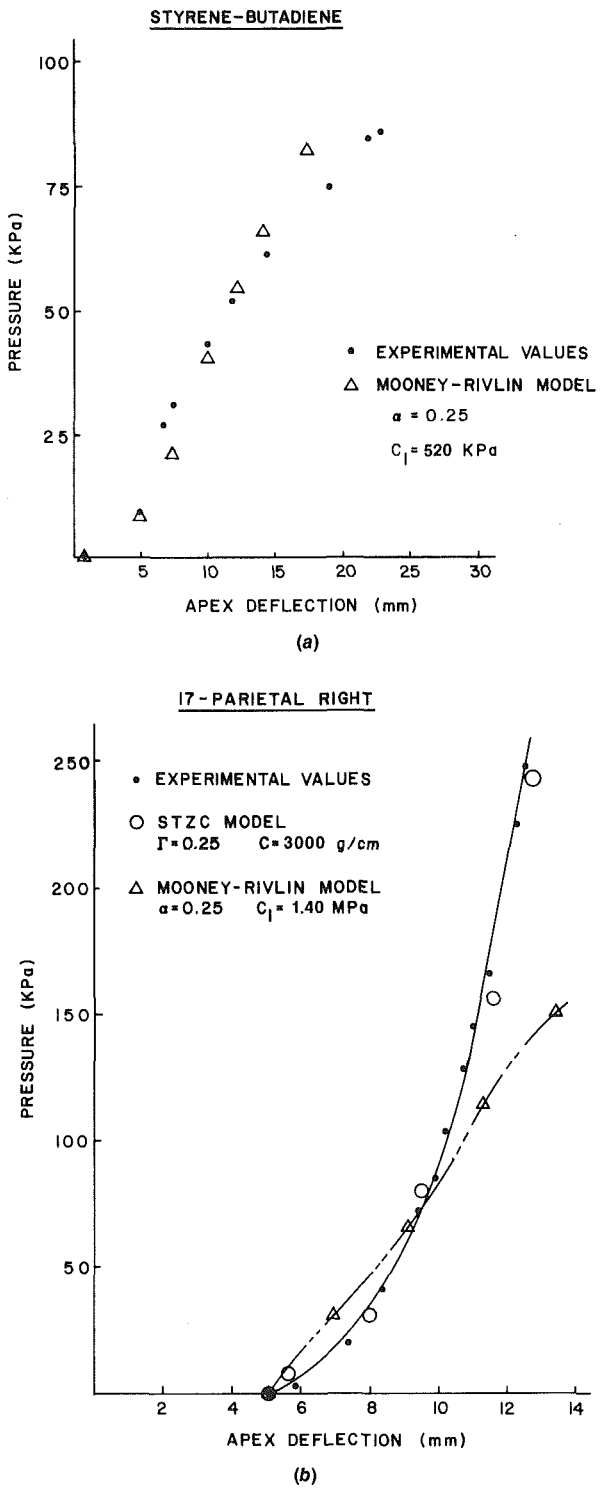

Fig. 6(a) The behavior of the Mooney-Rivlin material model was clearly adequate for characterizing the behavior of styrene-butadiene rubber; but (b) the STZC model was superior to the Mooney-Rivlin model in characterizing fetal dural mater where the latter diverged from the experimental response under large deflections. The dots represent the experimental values, the triangles are from the Mooney-Rivlin model and the open circles are from the STZC model.

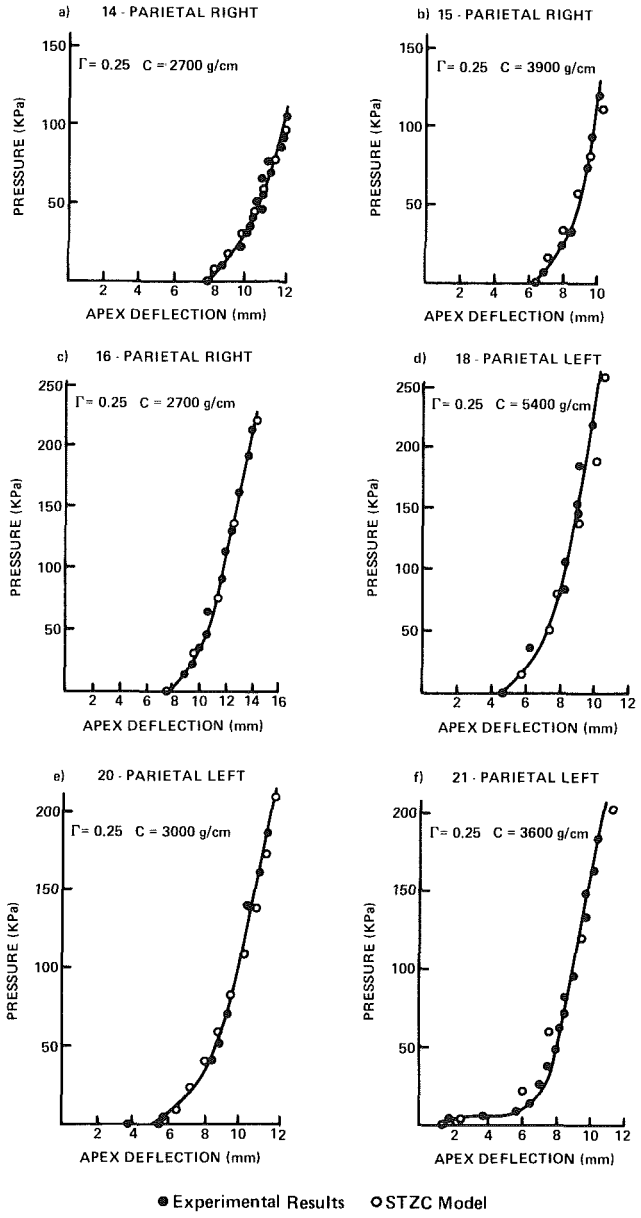

Fig. 7 A composite of several of the experimental and theoretical load-deflection curves is shown. The dots represent experimental values while the open circles are from the STZC model. Best results were obtained in all cases for Γ = 0.25. The material stiffness factor, C, for each inset is: (a) 2700g/cm, (b) 3900g/cm, (c) 2700g/cm, (d) 5400 g/cm, (e) 3000g/cm, and (f) 3600g/cm.

$$T_2 = \frac{2hC_1}{\lambda_1\lambda_2}(\lambda_2^2 - \bar{\lambda}_1^2\bar{\lambda}_2^2)(1+\alpha\lambda_1^2), \tag{17}$$

in which h is the initial, uniform thickness of the membrane, $\alpha = C_2/C_1$, and C_1 and C_2 are the material constants with the dimensions of stress. For the STZC model, the constitutive relations are

$$T_1 = \frac{C\lambda_1}{2\lambda_2}[\Gamma(\lambda_1^2 - 1) + \lambda_2^2(\lambda_1^2\lambda_2^2 - 1)], \tag{18}$$

$$T_2 = \frac{C\lambda_2}{2\lambda_1}[\Gamma(\lambda_2^2 - 1) + \lambda_1^2(\lambda_1^2\lambda_2^2 - 1)], \tag{19}$$

Table 2 The numerically determined values of the independent variables for the STZC model are listed

Specimen	Γ	C(g/cm)
14 – parietal left	0.25	2000
14 – parietal right	0.25	2700
15 – parietal right	0.25	3900
16 – parietal right	0.25	2700
17 – parietal right	0.25	3000
18 – parietal right	0.25	5400
19 – parietal left	0.25	4700
20 – parietal left	0.25	3000
21 – parietal left	0.25	3600

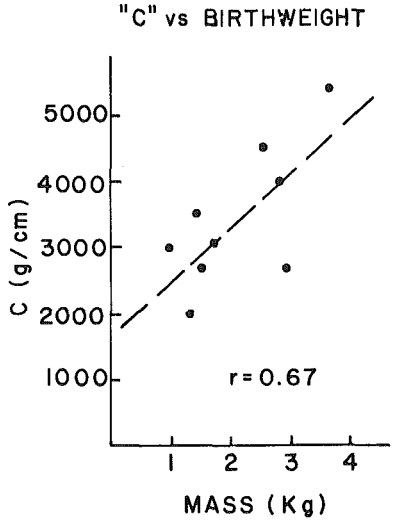

Fig. 8 A positive correlation existed between the material stiffness factor, C, and fetal development ($r = 0.67, p < 0.05$)

in which $\Gamma = B/C$, and B and C are the material constants with the dimensions of force per unit length. Equations (12)–(14) can be solved with the Runge-Kutta method [20]. The numerical integration starts at $r = 0$, and the generator of the membrane is divided into twenty equal meshes. The solution is completed under the requirement that the radius of the deformed membrane at the last mesh point must be equal to the initial outer radius which is actually the boundary conditions at that point.

Results

Figure 6 compares the experimental results with the response of the Mooney-Rivlin material model and the STZC material model. Figure 6(*a*) demonstrates that the Mooney-Rivlin model descibes well the behavior of the styrene-butadiene rubber (a = 0.25, C = 0.5 MPa). However, in the case of dura, Fig. 6(*b*) demonstrates that the behavior of the STZC model describes the biological material better than does the Mooney-Rivlin model, the latter of which diverges from the membrane's response for large apex deflections. The independent variables providing the best fit of the respective models are given in the figures. It is clear that the STZC model will consistently give a better fit to the experimental data.

Figure 7 presents the responses of the membranes measured not shown in other figures. Table 2 lists the computed values of the independent variables of the STZC model for all the tests.

For a standard set of initial conditions, the computed values of C were plotted against birthweight (Fig. 8). The correlation was statistically significant (r = 0.67, $p < 0.05$).

Comments

The limited availability of fetal dura mater precluded investigation of storage effects during this study; however, the two unfrozen specimens, tested within days of excision, exhibit loading curves within the scatter of the curves from the frozen specimens as can be seen in Fig. 7.

The STZC strain energy function requires two constants to specify the nonlinear behavior of one curve out of a family of curves. When varying one of constants, Γ, from 0.10 to 0.40, the STZC response changes only slightly. (The possible values for Γ are between zero and one.) Setting $\Gamma = 0.25$ for all tests consistently gave the best results.

The numerical procedure requires the specification of an initial apex deflection and a membrane thickness. The range of measured thicknesses from all specimens yielded the same numerical results, so the average thickness of all dura sheets was used for all tests. Furthermore, initial apex deflections with $\pm$ 1 mm yielded essentially the same curves for deflections greater than 35 percent of the initial deflection.

Because the styrene-butadiene tests gave strikingly similar results with our test protocol, and the numerical methods yielded consistent results with variables easily specified within error tolerances smaller than those required, we are confident the source of the stiffness variance is the material itself.

We expected the material stiffness would be dependent on fetal development; specifically, that a more mature fetus would have stiffer dura. Although our sample size is not large enough to make conclusive observations, Fig. 8 indicates that material stiffness is indeed directly dependent on the physical development of the fetus.

In summary, this study demonstrates that the shape of the load-deflection curve of fetal dura mater can be approximated by the strain energy function defined by Skalak and associates [19]. The effects of potentially confounding factors such as cause of death and membrane preparation, storage, and moisture content need to be studied to further reduce the variation in the computed stiffness values. Correlations between stiffness and other physiological variables, such as membrane thickness, may also be discovered.

Acknowledgments

This work was supported in part by NIH grant HD11202, and the Bioengineering Program of The University of Michigan. We gratefully acknowledge the support of Alan S. Wineman, Ph.D., during this study and the use of the Highway Safety Research Institute facilities.

References

1 Lillien, A. A., Term Intrapartum Fetal Death," *American Journal of Obstetrics and Gynecology*, Vol. 107, 1970, p. 595.

2 *A Report to the State Assembly on Developmental Disabilities in California*, Arthur Bolten Associates, Sacramento, Calif., 1972.

3 Quilligan, E. J., and Paul, R. H., Fetal, "Monitoring: Is It Worth It?" *Obstetrics and Gynecology*, Vol. 45, No. 1, 1975, pp. 96–100.

4 Fung, Y. C. B., "Stress-Strain-History Relations of Soft Tissues in Simple Elongation," *Biomechanics, Its Foundations and Objectives*, eds., Y. C. Fung, N. Perrone, and M. Anliker, Prentice-Hall, Inc., New Jersey, 1972, pp. 181–208.

5 Melvin, J. W., McElhaney, J. H., and Roberts, V. L., "Development of a Mechanical Model of the Human Head—Determination of Tissue Properties and Synthetic Substitute Materials," *Proceeding of the 14 Stapp Car Crash Conference*, Society of Automotive Engineers, Inc., New York, 1970.

6 Borell, U., and Fernstrom, I., Die Umformung des kindlichen Kopfes wahrend mormaler Entbindung in regelrechter Hinterhauptslage und bei engem Becken, *Gerburtsh u Frauenheilk*, Vol. 18, 1958, p. 1156.

7 Green, A. E., and Adkins, J. E., *Large Elastic Deformations*, 2nd Edition, Oxford University Press, London, 1970.

8 Feng, W. W., and Yang, W. H., "On the Contact Problem of an Inflated Spherical Nonlinear Membrane," *Journal of Applied Mechanics*, Vol. 40, 1973, pp. 202–214.

9 Yang, W. H., and Feng, W. W., "On Axisymmetrical Deformations of Nonlinear Membranes," *Journal of Applied Mechanics*, Vol. 37, 1970, pp. 1002–1011.

10 Benedict, R., Wineman, A., and Yang, W. H., "The Determination of Limiting Pressure in Simultaneous Elongation and Inflation of Nonlinear Elastic Tubes," *International Journal of Solids Structures*, Vol. 15, 1979, pp. 241–249.

11 Bogen, D. K., and McMahon, T. A., "Do Cardiac Aneurysms Blow Out?" *Biophysics Journal*, Vol. 27, 1979, pp. 301–316.

12 Alem, N. N., Melvin, J. W., and Holstein, G. L., "Biomedical Applications of Direct Linear Transformation in Close-Range Photogrammetry," *Proceedings of the 6 New England Bioeng. Conference*, ed., Dov Jardon, Pergamon Press, 1978.

13 Wineman, A. S., "Large Axisymmetric Inflation of a Nonlinear Viscoelastic Membrane by Lateral Pressure," *Transactions of the Society of Rheology*, Vol. 20, 1976, pp. 203–225.

14 Mohan, D., *Passive Mechanical Properties of Human Aortic Tissue*, Ph.D. dissertation, The University of Michigan, University Microfilms, Publ. No. 76-27550, 1976.

15 Wineman, A., Wilson, D., and Melvin, J. W., "Material Identification of Soft Tissue Using Membrane Inflation," *Journal of Biomechanics*, Vol. 12, 1979, pp. 841–850.

16 Decraemer, W. F., Maes, M. A., and Vanhuyse, V. J., "An Elastic Stress-Strain Relation for Soft Biological Tissue Based on a Structural Model," *Journal of Biomechanics*, Vol. 13, 1980, pp. 463–468.

17 Pujara, P., and Lardner, T. J., "Deformations of Elastic Membranes—Effect of Different Constitutive Relations," *Z. Angew. Math. Phys.*, Vol. 29, 1978, pp. 315–327.

18 Crisp, J. D. C., "Properties of Tendon and Skin," *Biomechanics, Its Foundations and Objectives*, eds., Y. C. Fung, N. Perrone, and M. Anliker, Prentice Hall, Inc. New Jersey, 1972, pp. 141–179.

19 Skalak, R., Tozeren, A., Zarda, R., and Chien, S., "Strain Energy Function of Red Blood Cell Membranes," *Biophysics Journal*, Vol. 13, 1973, pp. 245–264.

20 Ralston, A., and Wilf, H., *Mathematical Methods for Digital Computers*, Wiley, New York, 1960, pp. 110–120.